Combustion and Flame 162 (2015) 287–295

Contents lists available at ScienceDirect

Combustion and Flame

journal homepage: www.elsevier.com/locate/combustflame

A dynamic adaptive method for hybrid integration of stiff chemistry

Yang Gao [a], Yufeng Liu [a], Zhuyin Ren [b], Tianfeng Lu [a,*]

[a] Department of Mechanical Engineering, University of Connecticut, Storrs, CT 06269-3139, United States
[b] Center for Combustion Energy and School of Aerospace Engineering, Tsinghua University, Beijing 100084, China

ARTICLE INFO

Article history:
Received 28 April 2014
Received in revised form 24 July 2014
Accepted 24 July 2014
Available online 15 August 2014

Keywords:
Dynamic adaptive method for hybrid integration
Stiff chemistry solver
Operator splitting scheme
Strang splitting scheme
Computational singular perturbation

ABSTRACT

The operator-splitting schemes for integration of stiff diffusion–reaction systems were found to fail in error control, i.e. incurring $O(1)$ relative errors, with splitting time steps larger than that required for fully explicit integration, when significant non-chemical radical sources are present. It was shown that, by excluding the transport term from the chemistry integration, errors by orders of magnitude may occur in radical concentrations solved in the chemistry sub-step, resulting in significant errors in the major species. The failing scenario is demonstrated with a toy problem and an unsteady perfectly-stirred reactor (PSR) for hydrogen/air with significant H radical concentration at inlet. A dynamic adaptive method for hybrid integration (AHI) of stiff chemistry is then proposed as a substitute for the operator-splitting schemes in such cases. The AHI method can obtain accurate solutions by integrating the fast species and reactions implicitly and the non-stiff terms, including slow reactions and non-chemical source terms, explicitly. Specifically, fast species and reactions are identified on-the-fly based on their analytically derived timescales, the rates of slow variables are evaluated explicitly and those of fast species are evaluated partial-implicitly. As such, the number of variables to be implicitly solved at each integration time step is reduced to the number of the fast species, resulting in a smaller Jacobian matrix and consequently lower computational cost compared with the fully implicit solvers. The hybrid method is validated in auto-ignition for hydrogen/air with different equivalence ratios and initial temperatures, and compared with the Strang splitting scheme for the toy problem and the unsteady PSR. Results show significant improvement in accuracy using the AHI method.

1. Introduction

Detailed chemistry is important for high-fidelity reacting flow simulations. Major challenges to incorporate detailed chemistry in large-scale simulations are primarily attributed to the large sizes and severe stiffness of detailed chemistry. While detailed mechanisms can be reduced in size through skeletal reduction and timescale analyses [1], chemical stiffness renders the low-cost explicit integration solvers inapplicable for many flow simulations, particularly when relatively large time steps are adopted, and computationally expensive implicit solvers are typically required to integrate combustion problems. Chemical stiffness is induced by the extremely short timescales associated with highly reactive radicals and fast reactions. In direct numerical simulations (DNS) of compressible reacting flows, the time steps are typically limited by the fine spatial resolution and the Courant–Friedrichs–Lewy (CFL) condition, such that the typical step sizes for time-integration are smaller than, say, 10 ns [2], and in such cases chemical stiffness can be removed on-the-fly without significant overhead due to the sparse coupling of the fast chemical processes [3]. However, stiffness removal for simulations with significantly larger integration time steps remains a challenge due to the densely-coupled fast chemical processes, particularly the fast reactions that are in partial equilibria. While such timescale analyses as computational singular perturbation (CSP) [4,5] and intrinsic low dimensional manifold (ILDM) [6] can be employed to systematically eliminate the short timescales of fast modes, significant computational overhead is involved with the methods based on Eigen-analysis such that the overall computational time is comparable to or even higher than that using the implicit solvers, e.g. VODE [7] and DASAC [8],which are widely adopted in practical reacting flow simulations.

The computational overhead of implicit solvers is primarily attributed to the Jacobian evaluation and LU decomposition. As such, the computational cost is typically $O(n^2)$, where n is the number of species, for small to moderately large mechanisms where the Jacobian evaluation is through numerical perturbations and dominates the computational cost, and $O(n^3)$ for large mechanisms

* Corresponding author.
E-mail address: tlu@engr.uconn.edu (T. Lu).

http://dx.doi.org/10.1016/j.combustflame.2014.07.023
0010-2180/

where the LU decomposition is the most time consuming operation. Evaluation of the Jacobian matrix can typically be expedited through analytic techniques [1], and the high computational cost associated with LU decomposition can be reduced by preconditioning [9] and sparse matrix techniques [10–13], and linear scaling with large mechanisms for spatially homogenous reactor calculations was observed.

For simulations of multi-dimensional flows, fully implicit integration schemes typically induce high computational costs due to the large number of spatial grid points involved. Implicit–Explicit (IMEX) approaches combine implicit and explicit discretizations for different source terms for reduced computational cost [14–18]. Operator-splitting schemes [19–26] are frequently used to integrate stiff chemistry and non-chemical processes in separate sub-steps, such that the expensive implicit solvers are only invoked for the integration of local chemistry, while the low cost explicit solvers can be employed to integrate the non-chemical source terms. In particular, the Strang splitting scheme [26] is among the most widely used operator splitting schemes for practical combustion simulations. It features second-order accuracy for sufficiently small splitting time steps and is rather straightforward to implement. While error control of the splitting schemes has been well studied at the limit of small splitting time steps, the splitting time steps adopted in most practical simulations are typically moderately large to avoid excessively high computational cost, and such cases with moderately large splitting time steps are referred to as coarse cases [22]. Splitting errors induced by stiff chemistry in coarse cases can be rather large [27], although successes have been reported in many studies, e.g. [21,25,28]. The mechanisms for the large splitting errors in coarse cases can be complex and are not fully understood.

In the present study, a mechanism associated with stiff chemistry that can result in failed error control of operator-splitting schemes in coarse cases is identified. The reason of the failure is attributed to the significant modification of the slow chemistry's trajectory by operator splitting, i.e. by excluding the transport source term from the sub-step for chemistry integration. A dynamic adaptive method for hybrid integration (AHI) is then proposed as a substitute of the operator-splitting schemes to integrate combustion systems involving stiff chemistry with improved accuracy.

As the outline of this paper, the large splitting errors of the Strang splitting scheme in coarse cases are first demonstrated and investigated using a toy problem. An AHI method is then proposed to resolve this issue and to achieve accurate and efficient time-integration of stiff chemistry coupled with transport. The AHI method is tested in auto-ignition and the solutions are compared with that from SENKIN [29], which utilizes the fully implicit DASAC solver based on the backward difference formula (BDF). The results of AHI are then compared with that of the Strang splitting scheme for the toy problem and an unsteady perfectly stirred reactor (PSR) of hydrogen/air using detailed chemistry.

2. The Strang splitting scheme and a toy problem

The Strang splitting scheme is among the most widely used solvers for reacting flows involving stiff chemistry, for which the spatially discretized governing equations can be expressed as:

$$\frac{d\boldsymbol{\Phi}}{dt} = \boldsymbol{M}(\boldsymbol{\Phi}) + \boldsymbol{S}(\boldsymbol{\Phi}) \tag{1}$$

where $\boldsymbol{\Phi}$ is the vector of the thermo-chemical composition, including, e.g. temperature and species mass fractions. The operators $\boldsymbol{M}$ and $\boldsymbol{S}$ are for the transport and chemistry terms, respectively. To solve Eq. (1) using the second-order Strang splitting scheme [25,26], the time domain $[t_0, t_f]$ is discretized into n_t uniform intervals of size Δt, which are referred to as the splitting time steps. In each splitting time step, time-integration can be performed in the following sequence, namely the $\boldsymbol{S}/2 - \boldsymbol{M} - \boldsymbol{S}/2$ scheme:

$$\frac{d\boldsymbol{\Phi}^{(1)}}{dt} = \boldsymbol{S}\left(\boldsymbol{\Phi}^{(1)}\right), \quad \boldsymbol{\Phi}^{(1)}(0) = \boldsymbol{\Phi}^{n} \quad \text{on } [0, \Delta t/2] \tag{2a}$$

$$\frac{d\boldsymbol{\Phi}^{(2)}}{dt} = \boldsymbol{M}\left(\boldsymbol{\Phi}^{(2)}\right), \quad \boldsymbol{\Phi}^{(2)}(0) = \boldsymbol{\Phi}^{(1)}(\Delta t/2) \quad \text{on } [0, \Delta t] \tag{2b}$$

$$\frac{d\boldsymbol{\Phi}^{(3)}}{dt} = \boldsymbol{S}\left(\boldsymbol{\Phi}^{(3)}\right), \quad \boldsymbol{\Phi}^{(3)}(0) = \boldsymbol{\Phi}^{(2)}(\Delta t) \quad \text{on } [0, \Delta t/2] \tag{2c}$$

where $\boldsymbol{\Phi}^n$ is the composition at the beginning of the nth splitting time step. The initial conditions of Eqs. (2b) and (2c) are the solutions of Eqs. (2a) and (2b), respectively, and $\boldsymbol{\Phi}^{(3)}(\Delta t/2)$ is the solution at the end of the splitting time step. Eq. (2b) can typically be explicitly integrated in one step if the splitting time step is sufficiently small to resolve the transport term, while Eqs. (2a) and (2c) typically require multiple implicit steps using stiff ODE solvers. Note that one can build a $\boldsymbol{M}/2 - \boldsymbol{S} - \boldsymbol{M}/2$ scheme in a similar manner, which is nevertheless less accurate than the $\boldsymbol{S}/2 - \boldsymbol{M} - \boldsymbol{S}/2$ scheme as discussed in [22]. The $\boldsymbol{S}/2 - \boldsymbol{M} - \boldsymbol{S}/2$ scheme will be used to study the splitting errors in the following.

A toy model is first constructed to investigate the possible scenarios where the operator splitting schemes may fail in coarse cases. The model involves the following three reactions.

$$A \xrightarrow{k_1} R \tag{R$_1$}$$

$$R \xrightarrow{k_2} C \tag{R$_2$}$$

$$A + \alpha R \xrightarrow{k_3} B + \alpha R \tag{R$_3$}$$

where k_1, k_2 and k_3 are the reaction rate coefficients of reactions R$_1$, R$_2$, R$_3$, respectively. Species A is the reactant, B is the product, C is an intermediate species that is not of direct importance to A and B, and R is a radical that controls the important reaction (R$_3$) for product formation. The parameter α determines the overall reaction order and nonlinearity of (R$_3$).

For simplicity, the transport term of species R is set to be a constant, d, and those for the other species are set to be zero. The term d mimics the effect of a mixture, e.g. in the preheat zone of a premixed flame, receiving substantial amount of radicals from a neighboring fluid element, e.g. in the reaction zone. Note that including nontrivial transport terms for the major species does not affect the nature of the toy problem.

The dependent variables and source terms in Eq. (1) for the toy problem can thereby be expressed as:

$$\begin{aligned} &\boldsymbol{\Phi} = [A, B, C, R]^T, \\ &\boldsymbol{S} = [-k_1 A - k_3 A R^{\alpha}, k_3 A R^{\alpha}, k_2 R, k_1 A - k_2 R]^T, \\ &\boldsymbol{M} = [0, 0, 0, d]^T, \end{aligned} \tag{3}$$

with the initial condition being

$$A = 1, B = C = R = 0, \quad \text{at } t = 0$$

k_2 is chosen to be much larger than k_1, i.e. $k_2 \gg k_1$, such that R stays in quasi steady state (QSS) after an initial transient period and can be approximated as

$$R \approx \frac{k_1 A + d}{k_2} \tag{4}$$

and the timescale of R can be defined as $\tau = 1/k_2$. It is seen that the concentration of R is sensitive to transport unless $|d| \ll k_1 A$.

However, without the transport term, the concentration of R in the chemistry sub-step in Eqs. (2a) and (2c) after an initial transient period can be approximated as

$$R \approx \frac{k_1 A}{k_2} \tag{5}$$

which can be significantly different from that in Eq. (4) if d is not trivial, resulting in large errors in the reaction rate of (R_3). The error in the chemistry sub-step can subsequently lead to significant splitting errors in the major species as demonstrated in the following cases.

The following parameters are used for the toy problem in all the simulations in the present study unless particularly specified: $k_1 = 1$, $k_2 = \tau^{-1} = 10^6$, $k_3 = \tau^{-\alpha}$, $d = 1$, while different values of α and the splitting time step Δt are used. Note that k_3 is selected such that the rate of reaction (R_3) is $O(1)$. To measure the splitting errors, the "exact" solutions for this toy model are obtained using fully implicit integration with sufficiently small time steps such that the numerical error is negligible for the measurement.

Figure 1 shows the profiles of A, B and R in the toy model with $\alpha = 2$. It is seen that the splitting scheme with $\Delta t = 10^{-7}$ agrees well with the exact solution because Δt is sufficiently small to resolve radical R whose timescale is $\tau = 10^{-6}$, i.e. the problem is not stiff at such a small splitting time step. However, when a larger splitting time step, $\Delta t = 10^{-5}$, is used, which should nevertheless still be sufficiently small to accurately resolve the major species profiles, which have timescales of $O(1)$, large errors occur for all the species. The error in R is primarily induced by the mechanism explained in Eqs. (4) and (5), and the errors in A and B can only be attributed to the error in R because the transport terms are trivial for A and B.

Figure 2 shows the relative errors in the concentrations of B and R, respectively, as functions of the splitting time step Δt for $\alpha = 2$, with the dotted line indicating the trend line of slope 2. In the present study, the relative error, ε, in a computed quantity, ψ, is defined as

$$\varepsilon = \frac{|\psi - \psi^E|}{|\psi + \psi^E|} \tag{6}$$

where ψ^E is the value from the exact solution. The relative errors in Fig. 2 for the Strang splitting scheme is measured at the time when $A = 0.5$ in the exact solution for the toy problem. It is seen that when Δt is smaller than the radical timescale, $\tau = 10^{-6}$, the Strang splitting scheme is second-order in accuracy. However, with $\Delta t \gg \tau$, e.g. $\Delta t = 10^{-5}$, the error control fails and the relative errors quickly approach $O(1)$. It is worth mentioning again that a time step of 10^{-5} is an unnecessarily small time step size to resolve the species profiles with non-splitting schemes, as to be shown in Section 4.2.1.

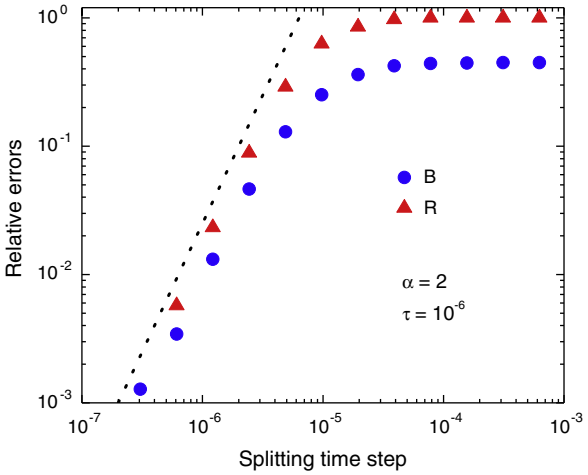

Fig. 2. Relative errors in species concentrations for the toy problem with $\alpha = 2$, measured at the time when $A = 0.5$ in the exact solution, as functions of the splitting time step for the second-order Strang splitting scheme. Dotted line shows the trend line with slope of 2.

To further investigate the dependence of the splitting error on the nonlinearity of the toy problem, as characterized by the parameter α, Fig. 3 shows the relative errors of the Strang splitting scheme in species concentrations measured at time when $A = 0.5$ in the exact solution for different α values. It is interesting to observe that while large errors are present for the strongly nonlinear cases, e.g. $\alpha = 2$, the errors in A and B vanish when the problem becomes quasi-linear in R, that is $\alpha = 1$. The reason for the small, or precisely zero, error in A and B at $\alpha = 1$ is attributed to the exact error cancellation, which also occurs when the operators are commuting in special cases [22]. It is noted that the splitting error changes sign at $\alpha = 1$. For the present toy problem, while errors in A and B vanish in the quasi-linear case, the error in R remains large such that the operators are not commuting. To scrutinize the process of the error cancellation in B, Fig. 4 plots the concentrations of B and R within the first splitting time step $[0, \Delta t]$ for the cases with (a) $\alpha = 2$, (b) $\alpha = 1$, respectively, with $\Delta t = 10^{-4}$. It is seen in Fig. 4(b) that while large errors in the concentration of B are

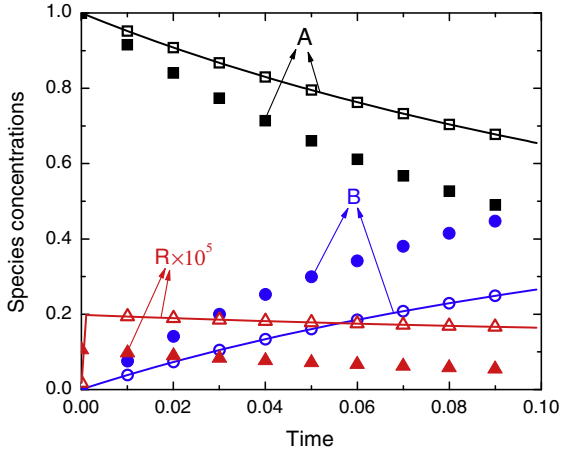

Fig. 1. Calculated species concentration profiles for the toy problem with $\alpha = 2$ and $\tau = 10^{-6}$. Lines: exact solution; Closed symbols: Strang splitting scheme with $\Delta t = 10^{-5}$; Open symbols: Strang splitting scheme with $\Delta t = 10^{-7}$.

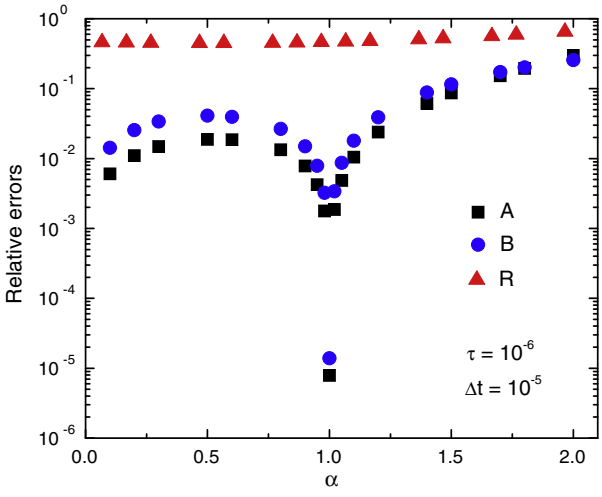

Fig. 3. Relative errors in species concentrations for the toy problem, measured at the time when $A = 0.5$ in the exact solution, as functions of α, for the Strang splitting scheme with $\Delta t = 10^{-5}$.

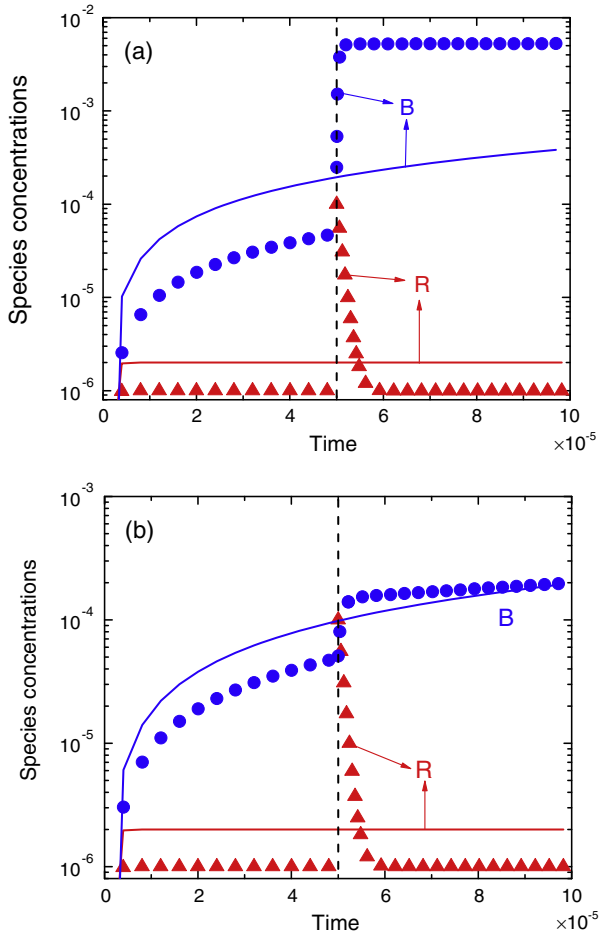

Fig. 4. Concentrations of B and R calculated with the Strang splitting scheme with $\Delta t = 10^{-4}$ for the toy problem with (a) $\alpha = 2$ and (b) $\alpha = 1$. The solid lines indicate the exact solutions and markers indicate the Strang splitting scheme. The dash line indicates the end of integration of Eq. (2a) and the beginning of integration of Eq. (2c). The jump in R results from the integration of Eq. (2b).

present in the chemistry sub-steps for Eqs. (2a) and (2c), the errors cancel exactly at the end of the splitting time step for $\alpha = 1$. In contrast, the errors only cancel partially for the cases with $\alpha = 2$. It is noted again that the concentration of R cannot be accurately computed by the operator-splitting scheme regardless of the α values.

Based on the above observation, since nonlinearity is intrinsic in detailed chemistry, operator splitting schemes may subject to large splitting errors when significant radical sources from the transport term are present, e.g. for a mixture in the preheat zone of a premixed flame receiving H radicals from the reaction zone through back-diffusion.

3. A dynamic adaptive method for hybrid integration

To resolve this problem, an AHI method is proposed in the present study. The AHI method first separates the fast species and reactions from the slow ones by comparing their timescales with the integration time step. The fast chemical processes are integrated implicitly while the slow chemical processes and transport are integrated explicitly. The slow processes are always carried during the integration of the fast chemistry.

3.1. Identification of fast and slow reactions and species

A critical component in the AHI method is to identify fast and slow reactions and species on-the-fly. While CSP, ILDM and other Eigen-analyses could be used for fast-slow separation, efficiency is key for on-the-fly identification. An efficient criterion proposed by Lam [5] is used in the present study to define the timescale of a reaction:

$$\begin{aligned} &\tau_i \equiv |\mathbf{J}_i \cdot \boldsymbol{v}_i|^{-1} \\ &\mathbf{J}_i = \frac{\partial \Omega_i}{\partial \boldsymbol{c}} = \left[\frac{\partial \Omega_i}{\partial c_1}, \frac{\partial \Omega_i}{\partial c_2}, \cdots \frac{\partial \Omega_i}{\partial c_{n_s}}\right], \\ &\boldsymbol{v}_i = \left[v_{1,i}, v_{2,i}, \ldots v_{n_s,i}\right]^T, \end{aligned} \tag{7}$$

where Ω_i is the net reaction rate for the ith reaction, $\boldsymbol{c}$ is the vector of species mole concentrations, $v_{k,i}$ is stoichiometric coefficient of the kth species in the ith reaction, and n_s is the total number of species. The ith reaction is considered fast if

$$\tau_i < \frac{\tau_c}{\beta} \tag{8}$$

where τ_c is a threshold timescale which is set equal to the integration time step h in the present study, and β is a safety factor that can be mechanism dependent. The kth species is considered fast if it contributes significantly to a fast reaction, as determined by

$$\left|\frac{\partial \Omega_i}{\partial c_k}\right| > \beta \tau_c^{-1} \tag{9}$$

A value of $\beta = 0.5$ is used in the present study for all the simulations unless otherwise specified.

In the present study, the Jacobian of each reaction in Eqs. (7) and (9) is evaluated based on analytically derived derivatives to ensure high precision and efficiency. It is noted that temperature is always treated as a slow variable in the AHI method. To ensure the validity of this treatment, the integration time step must be sufficiently small to explicitly resolve heat release.

3.2. A dynamic adaptive method for hybrid integration

At any time instance during the integration, fast species and reactions can be identified based on Eqs. (7)–(9) using the current solution from Eq. (1), which can be rewritten as

$$\frac{d\boldsymbol{\Phi}}{dt} = \boldsymbol{S}_f + \boldsymbol{g}_s, \quad \boldsymbol{\Phi} = \begin{bmatrix} \boldsymbol{\Phi}_f \\ \boldsymbol{\Phi}_s \end{bmatrix} \tag{10}$$

where $\boldsymbol{\Phi}_f$ indicates the vector of variables for the fast species, and $\boldsymbol{\Phi}_s$ includes the slow species and other slow variables, e.g. temperature. It is emphasized again that the integration time step must be sufficiently small to resolve the temperature profile such that temperature is always a slow variable to be included in $\boldsymbol{\Phi}_s$. The source term $\boldsymbol{S}_f$ is the contribution from the fast reactions and $\mathbf{g}_s$ includes the contributions from both the slow reactions and the transport term, i.e.

$$\boldsymbol{S}_f = \sum_{i=1}^{m} \boldsymbol{v}_i \Omega_i \tag{11a}$$

$$\mathbf{g}_s = \sum_{i=m+1}^{n_r} \boldsymbol{v}_i \Omega_i + \boldsymbol{M} \tag{11b}$$

where n_r is the total number of reactions and m is the number of fast reactions, which are always listed before the slow ones.

For numerical integration, Eq. (10) can be discretized with a first-order scheme:

$$\frac{\Phi_i^{n+1} - \Phi_i^n}{h} = S_{i,f}(\boldsymbol{\Phi}_f^{n+1}, \boldsymbol{\Phi}_s^n) + g_{i,s}(\boldsymbol{\Phi}_f^n, \boldsymbol{\Phi}_s^n) \tag{12}$$

where the superscripts indicate the integration step number, the subscript i indicates the ith entry in $\boldsymbol{\Phi}$, and h is the time step size. It is seen that the contribution from the fast reactions, $\boldsymbol{S}_f$, is

evaluated partial-implicitly, while the slow reactions and the transport term in $\mathbf{g}_s$ are evaluated fully explicitly. To integrate Eq. (12), $\mathbf{\Phi}_f^{n+1}$ is first solved implicitly using the first N_f equations in Eq. (12) using the BDF scheme, where N_f is the length of vector $\mathbf{\Phi}_f$. The remaining N_s equations in Eq. (12), where N_s is the length of $\mathbf{\Phi}_s$, are then integrated explicitly using the forward Euler scheme to obtain $\mathbf{\Phi}_s^{n+1}$. It is noted that, in rare cases, the criteria in (8) and (9) may result in fast reactions involving no fast species. This will not incur accuracy or stability issues to the method since a reaction can be included in the $\boldsymbol{S}_f$ term whether it is fast or not.

Using the above procedure, the number of variables to be implicitly solved is reduced to the number of fast species, such that the computational cost of AHI can be significantly lower than that of the fully implicit chemistry solvers. In addition, the computational cost is further reduced since only the fast reaction rates need to be re-evaluated during the Newton iterations to solve the equations for the fast species, and there is no need to re-evaluate the slow reaction rates and the transport term during the iterations. As such, the computational cost of AHI is expected to be comparable to, or lower than, that of the operator splitting schemes and other fully implicit chemistry solvers.

4. Results and discussion

4.1. Accuracy and efficiency of the AHI method

The accuracy of the AHI method is first studied in constant-pressure auto-ignition, for which Eq. (1) can be expressed as

$$\mathbf{\Phi} = [Y_1, Y_2, \ldots Y_{n_s}, T]^T \tag{13a}$$

$$S_i(\mathbf{\Phi}) = \frac{\dot{m}_i}{\rho}, \quad i = 1, 2, \ldots n_s;$$

$$S_{n_s+1}(\mathbf{\Phi}) = -\frac{\sum_{i=1,n_s} \dot{m}_i h_i}{\rho c_p}, \quad \dot{m}_i = \omega_i W_i \tag{13b}$$

$$\boldsymbol{M}(\mathbf{\Phi}) = 0 \tag{13c}$$

where the subscript i indicates the ith species, ρ is density, T is temperature, Y_i, h_i, W_i and ω_i are mass fraction, specific enthalpy, molecular weight and the mole production rate, respectively, and c_p is the mixture averaged specific heat capacity. It is noted that the transport term is trivial for auto-ignition, and operator splitting is not involved in this Section for the test of the AHI method unless otherwise specified.

Figure 5 shows the numerical solutions of the constant-pressure auto-ignition for a stoichiometric hydrogen/air mixture, calculated with the fully explicit first-order Euler scheme, fully implicit (DASAC), and the AHI method, respectively. In the present work, the relative and absolute error tolerances for DASAC are set as 10^{-8} and 10^{-20}, respectively. The detailed hydrogen/air mechanism by Li et al. [30] with 9 species and 21 reactions is adopted. For comparison, the solution from the fully implicit solver is regarded as the exact solution. It is shown that the solution obtained by the AHI method with $h = 10^{-7}$ s agrees well with the exact solution, while the explicit solver with a smaller time step $h = 10^{-8}$ s diverges when ignition occurs, due to the extremely short timescales emerged near the ignition point as shown in Fig. 6. It is seen in Figs. 5 and 6 that the divergence occurs shortly after the shortest reaction timescale becomes smaller than the explicit integration time step, as indicated by the vertical dashed line. Figure 6 further shows that the shortest reaction timescale defined in Eq. (7) decreases rapidly from longer than 100 ns to shorter than 3 ns after the ignition, where temperature becomes higher than 2000 K. As such, the integration time of $h = 10^{-8}$ s is not sufficiently small for the explicit integration to be stable.

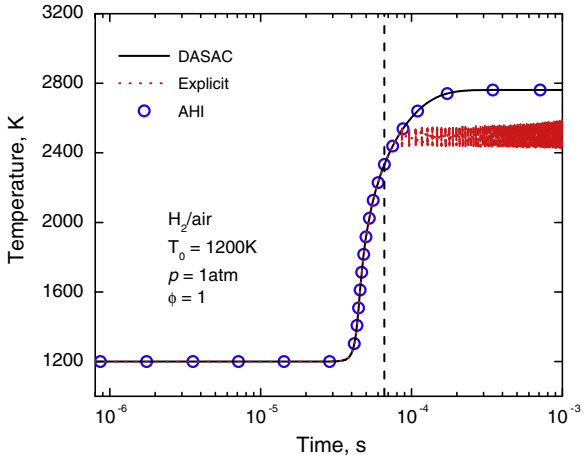

Fig. 5. Temperature profiles of constant-pressure auto-ignition of stoichiometric hydrogen/air, calculated using the fully implicit solver DASAC (solid line), AHI method with $h = 10^{-7}$ s (circles), and explicit first-order Euler scheme with $h = 10^{-8}$ s (dots), respectively. The vertical dashed line indicates when the fastest reaction timescale becomes smaller than the explicit integration time step.

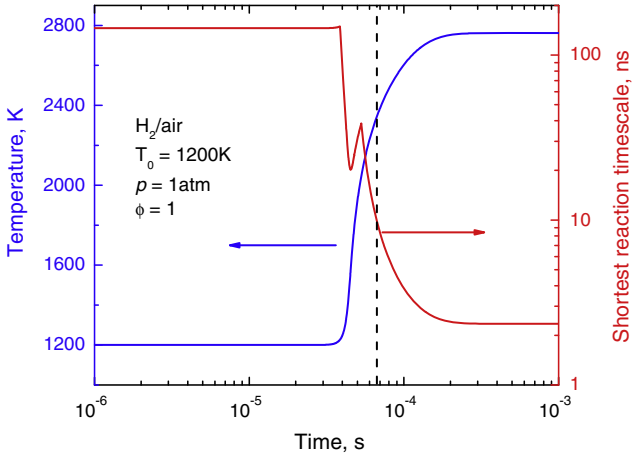

Fig. 6. The shortest reaction timescale and temperature profile as functions of time for constant-pressure auto-ignition of hydrogen/air. The vertical dashed line indicates when the fastest reaction timescale becomes smaller than the explicit integration time step.

Figure 7 further shows the detailed profiles of species mass fractions and the relative errors calculated using Eq. (6) in species mass fractions for auto-ignition of hydrogen/air. It is seen that with a fixed time step of $h = 10^{-7}$ s, the solutions from the AHI method agree well with that from DASAC, including the solutions near the ignition point, where the species mass fractions and temperature change dramatically. The ignition delays of hydrogen/air at different initial temperatures are further computed using DASAC and the AHI method, respectively, as shown in Fig. 8. It is seen that the results from the AHI method with a fixed time step of $h = 10^{-7}$ s are nearly identical to that of DASAC. The accurate and stable solutions by AHI using $h = 10^{-7}$ s for the different cases indicate that the fast chemical processes are effectively identified using the criteria in Eqs. (7)–(9).

To validate the order of accuracy of the AHI method, the dependence of local relative errors, defined in Eq. (6), of the AHI method on the integration time step size is measured for auto-ignition of stoichiometric hydrogen/air at atmospheric pressure, with initial temperature of $T_0 = 1200$ K. It is noted that in the present error measurements, only one integration step of size h is invoked for

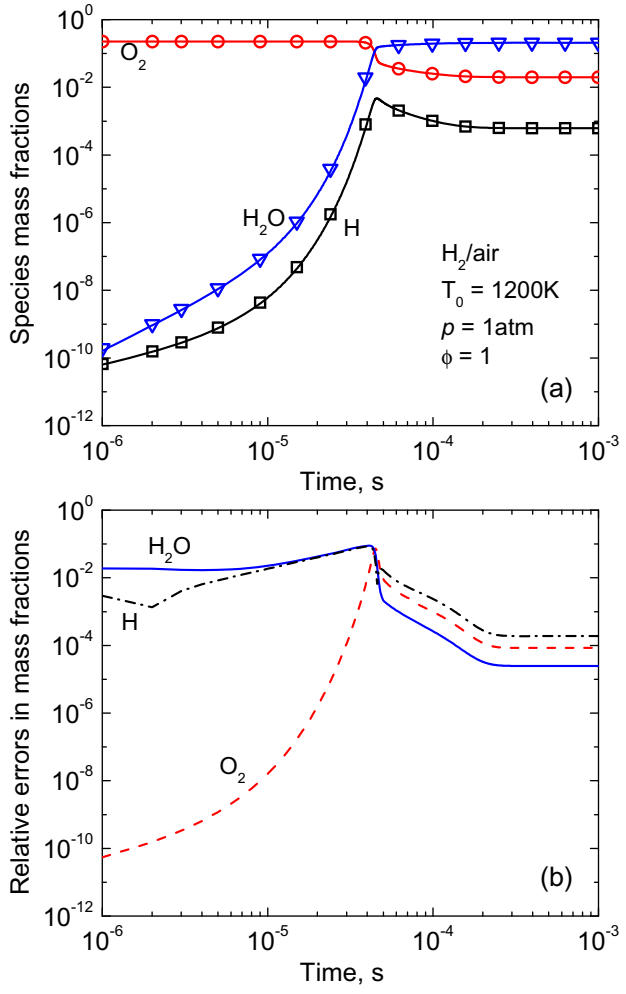

Fig. 7. (a) Profiles of species mass fractions for constant-pressure auto-ignition of hydrogen/air, calculated using DASAC (solid lines) and the AHI method with $h = 10^{-7}$ s (symbols), respectively. (b) Relative errors in species mass fractions between AHI and DASAC.

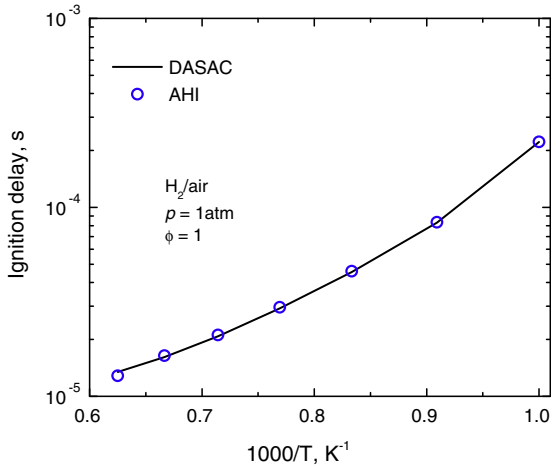

Fig. 8. Ignition delay of constant-pressure auto-ignition as a function of the initial temperature for stoichiometric hydrogen/air, calculated using DASAC (solid line) and the AHI method with $h = 10^{-7}$ s (circles), respectively.

each measurement. The integrations for both the AHI method and the exact solution start from the same initial condition, such that the measured error is strictly incurred by the single integration step. Furthermore, to ensure that the change in the measured quantity is not numerically trivial within the integration time step, the measurement is made near the ignition point, i.e. the inflection point of the temperature profile, where most dramatic changes occur in the variables. The measured relative errors of different variables are plotted in Fig. 9. It is seen that the single-step error of the first-order AHI method is of $O(h^2)$, and thus the method is confirmed to be overall first-order in accuracy. It is noted that the construction of higher-order schemes with dynamic adaptive fast-slow separation merits further investigation.

Compared with fully implicit solvers for chemistry integration, time savings can be achieved by the AHI method by reducing the number of fast variables to be solved implicitly. Figure 10(a) shows the number of fast species identified using Eqs. (7)–(9) at different temperatures in constant-pressure auto-ignition of hydrogen/air, ethylene/air and methane/air mixtures, respectively, at atmospheric pressure and initial temperature of $T_0 = 1200$ K. The simulations for ethylene/air and methane/air employ a 32-species skeletal mechanism [31] and a 111-species detailed mechanism [32], respectively, to show the fraction of fast variables in typical hydrocarbon flames. It is seen that the number of fast species is significantly smaller than the total number of species at low temperatures before the ignition points for all the cases. Considering that the computational cost of implicit solvers with dense Jacobian operations is a quadratic to cubic function of the number of variables, significant savings in computational cost can be achieved with the AHI method compared with the fully implicit methods when the mechanism is large. Figure 10(b) shows the CPU time for the overall simulation of constant pressure auto-ignition without transport and constant pressure unsteady PSR with transport, respectively.

For constant pressure unsteady PSR, the dependent variable list and the source terms of Eq. (1) for the unsteady PSR can be expressed as

$$\mathbf{\Phi} = [Y_1, Y_2, \ldots Y_{n_s}, T]^T \tag{14a}$$

$$S_i(\mathbf{\Phi}) = \frac{\dot{m}_i}{\rho}, \quad i = 1, 2, \ldots n_s,$$
$$S_{n_s+1}(\mathbf{\Phi}) = -\frac{\sum_{i=1,n_s} \dot{m}_i h_i}{\rho c_p}, \quad \dot{m}_i = \omega_i W_i \tag{14b}$$

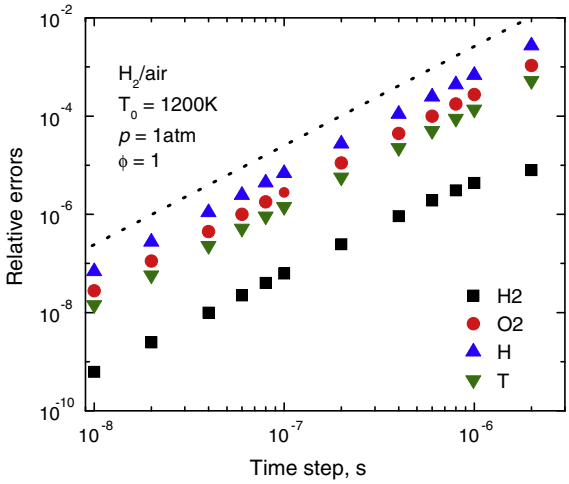

Fig. 9. Dependence of local relative errors on the integration time step size for constant-pressure auto-ignition of stoichiometric hydrogen/air. Dotted line: trend line with slope of 2. Symbols: measured relative errors.

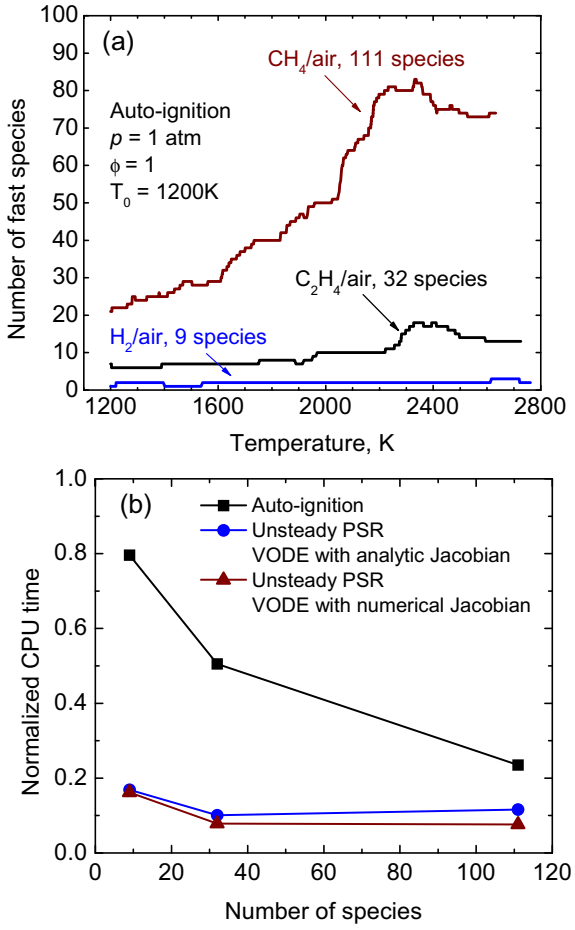

Fig. 10. (a) Number of fast species in constant-pressure auto-ignition, and (b) CPU time for the integration constant-pressure auto-ignition, normalized by that of fully implicit integration, and for unsteady PSR, normalized by that of the Strang splitting scheme using VODE, for hydrogen, ethylene and methane/air mixtures, respectively, at atmospheric pressure.

$$M_i(\mathbf{\Phi}) = \frac{Y_i^0 - Y_i}{\tau_{res}}, \quad i = 1, 2, \ldots n_s,$$
$$M_{n_s+1}(\mathbf{\Phi}) = \frac{\sum_{i=1,n_s} Y_i^0 (h_i^0 - h_i)}{c_p \tau_{res}} \tag{14c}$$

$$\tau_{res} = \frac{\rho V}{\dot{m}_{in}} \tag{14d}$$

where the superscript 0 indicates the inlet condition, V is the volume of the reactor, and τ_{res} is the residence time defined based on the inlet mass flow rate $\dot{m}_{in}$.

For the auto-ignition cases, the CPU time of the AHI method is normalized by the corresponding CPU time if all the species and reactions are treated implicitly in AHI. For the unsteady PSR cases, the CPU time of AHI method is normalized by the corresponding CPU time of the Strang splitting scheme where Eqs. (2a) and (2c) are solved using VODE with analytic and numerical Jacobian, respectively. It is noted that the AHI method in the present paper always uses analytic Jacobian. The simulation was measured for hydrogen/air, methane/air and ethylene/air at atmospheric pressure. The auto-ignition cases were initialized with stoichiometric fuel/air mixtures at $T_0 = 1200$ K, while the unsteady PSR is initialized with the steady state solution with temperature perturbed by +10 K such that the PSR relaxes toward the steady state solution during the integration. The inlet stream of the PSR consists of fresh stoichiometric fuel/air mixtures at $T_{in} = 300$ K, and the residence time is $\tau_{res} = 1$ ms. All the cases are integrated from $t = 0$ to 0.05 s with fixed time steps of 10^{-7} s, and the system has mostly reached steady state at the end of the integration. β is chosen to be 0.4 for the methane/air case, while the default value of 0.5 was used for the other cases. It is seen that the AHI method achieves approximately 20%, 40%, and 70% time savings for hydrogen, ethylene and methane cases, respectively, for the auto-ignition cases. The time savings are primarily attributed to the reduced number of fast variables that are implicitly solved. In contrast, time savings by factors of 5–10 were achieved for the unsteady PSR cases compared to the splitting scheme using VODE and analytic Jacobian, and even larger time savings were achieved compared to the splitting scheme with Jacobian evaluated through numerical perturbations. The significant time savings for unsteady PSR are primarily attributed to the nontrivial transport term in Eq. (14). In the splitting scheme, many integration steps are invoked at the beginning of each chemistry sub-step to resolve the relaxation of the fast chemical modes that are artificially activated when the transport term is switched on or off, as demonstrated in Fig. 4 for radical R in the toy problem, while the AHI method does not involve the artificial activation of the fast chemical modes because the transport term is always integrated with chemistry. As such, the current AHI method can be substantially more efficient than the splitting schemes even if adaptive fast chemistry is not used, i.e. all the species and reactions are treated implicitly. The measurement of computational cost was based on numerical codes implemented in FORTRAN and compiled with the Intel FORTRAN Compiler on Intel CPUs.

4.2. Comparisons of the AHI method and the Strang splitting scheme

4.2.1. Comparison for the toy problem

The performance of the AHI method is first compared with the operator-splitting scheme for the toy problem in Section 2. To solve the toy problem with the AHI method, the integration time step sizes are selected such that (R_1) and (R_3) are slow reactions, and (R_2) is a fast reaction. A, B and C are slow species solved explicitly, and R is a fast species solved implicitly.

Figure 11 shows the solutions from the AHI method and the Strang splitting scheme, respectively, in comparison with the exact solution obtained with a sufficiently small integration time step. A splitting time step of $\Delta t = 10^{-5}$ is used for the splitting scheme, and a time step of $h = 10^{-5}$ is used for AHI. It is observed that the AHI method can accurately solve the case while the Strang splitting scheme results in $O(1)$ errors in all the species. Figure 12 further shows the relative errors in B as functions of the splitting time step Δt for the Strang splitting scheme, and the integration time step h for the AHI method, respectively. The relative errors for both methods are measured at time when $A = 0.5$ in the exact solution. The dotted line and the dashed line are the trend lines with slope of 2 for the splitting scheme and slope of 1 for AHI, respectively. It is demonstrated that for the Strang splitting scheme, the point where the method starts to show the desired second-order behavior strongly depends on, and is close to, the timescale of radical R. Specifically, in the cases with $\tau = 10^{-8}$ and $\tau = 10^{-6}$, the splitting errors barely decrease until the splitting time step is shorter than approximately 10^{-7} and 10^{-5}, respectively. Note that explicit solvers can be used to integrate the toy problem with a time step close to or shorter than τ. Furthermore, the splitting time step Δt in the Strang splitting scheme is different from the integration time step h in the AHI method, as each chemistry integration sub-step of the operator-splitting scheme consists of a sequence of fractional implicit integration steps much smaller than Δt. Within each chemistry sub-step, multiple internal implicit integration time steps are typically involved when using stiff ODE solvers to solve Eqs. (2a) and (2c), as discussed in the previous section for the unsteady PSR. In

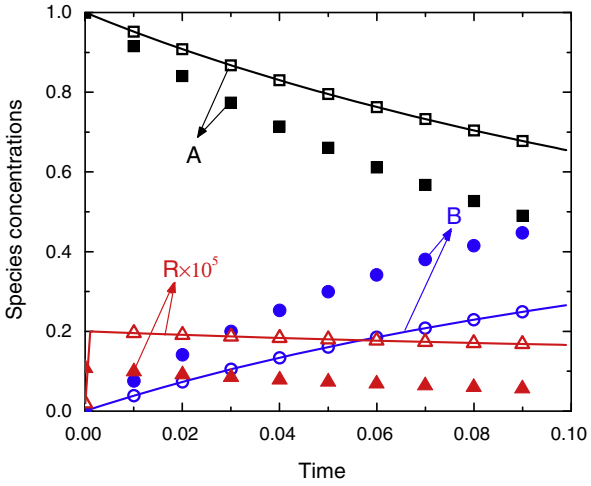

Fig. 11. Profiles of species concentrations in the toy problem with $\alpha = 2$ and $\tau = 10^{-6}$, calculated with the AHI method with $h = 10^{-5}$ (open symbols) and the Strang splitting scheme with $\Delta t = 10^{-5}$ (closed symbols), respectively, in comparison with the exact solution (lines).

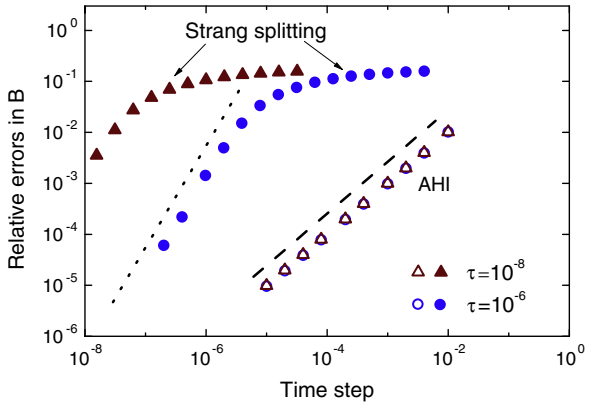

Fig. 12. Relative errors in B for the toy problem, measured at time when $A = 0.5$ in the exact solution, as functions of the time step, i.e. Δt for the Strang splitting scheme and h for AHI, with $\alpha = 0.5$ for cases with different timescales of R. Closed symbols: Strang splitting scheme. Open symbols: AHI. Triangles: $\tau = 10^{-8}$, circles: $\tau = 10^{-6}$. The dotted trend line has slope of 2 and the dashed line has slope of 1.

comparison, an integration time step in AHI does not consist of any additional sub-step. Therefore it makes no sense in terms of computational cost to integrate the toy problem using splitting schemes with a splitting time step close to or shorter than τ.

In comparison, the relative errors in B using the AHI method are mostly independent of τ for the two cases, and are smaller than that of the splitting scheme by orders of magnitude at a reasonable time step for implicit solvers, e.g. 10^{-2}–10^{-5}, considering that the timescales of the major species are $O(1)$.

4.2.2. Comparison for an unsteady PSR

The AHI method is further compared with the Strang splitting scheme with an unsteady PSR of hydrogen/air with significant source of H radical at inlet. The unsteady PSR is initialized with fresh H_2/air mixture at $\phi = 0.3$ and temperature of 875 K. The inlet stream consists of fresh H_2/air mixture at $\phi = 0.3$ enriched with 0.1% (in mass) H radical. The inlet condition is time independent with temperature of $T_{in} = 875$ K. Pressure of the reactor is fixed at $p = 80$ atm and residence time is fixed at $\tau_{res} = 2 \times 10^{-6}$ s. For integration of the PSR with the Strang splitting scheme, the chemistry sub-step is solved fully implicitly while the transport sub-step is solved explicitly using the second-order Runge–Kutta method. The exact solution is obtained by a fully implicit solver without operator splitting.

Figure 13(a) compares the results from the AHI method with $h = 2 \times 10^{-7}$ s and the Strang splitting method with $\Delta t = 2 \times 10^{-7}$ s, respectively. It is observed that the mixture ignites approximately at $8\tau_{res}$ as indicated by the exact solution and the solution from AHI, while the Strang splitting scheme predicts an ignition time of approximately $15\tau_{res}$. To further demonstrate the source of the error in the Strang splitting scheme, Fig. 13(b) shows that the calculated H mass fraction and the normalized contribution of the transport term as a fraction of the creation rate of H radical, F_H, which is expressed as

$$F_H(\mathbf{\Phi}) = M_H(\mathbf{\Phi})/[M_H(\mathbf{\Phi}) + C_H(\mathbf{\Phi})] \tag{15a}$$

$$C_H(\mathbf{\Phi}) = \sum_{i=1}^{n_r} (\nu^f_{H,i}\Omega^r_i + \nu^r_{H,i}\Omega^f_i) \tag{15b}$$

where M_H is the transport term for H radical calculated by Eq. (14c), C_H is the chemical creation rate of H. The subscript i indicates the ith reaction, $\nu^f_{H,i}$ and $\nu^r_{H,i}$ are the forward and reverse stoichiometric coefficients of H in the ith reaction, respectively, and Ω^f_i and Ω^r_i are the forward and reverse reaction rates, respectively. It is seen that the Strang splitting scheme significantly under-predicts the H mass fraction in the early stage of the ignition, where the contribution of the H radical from the transport term dominates the chemical creation rate, through the same mechanism explained in

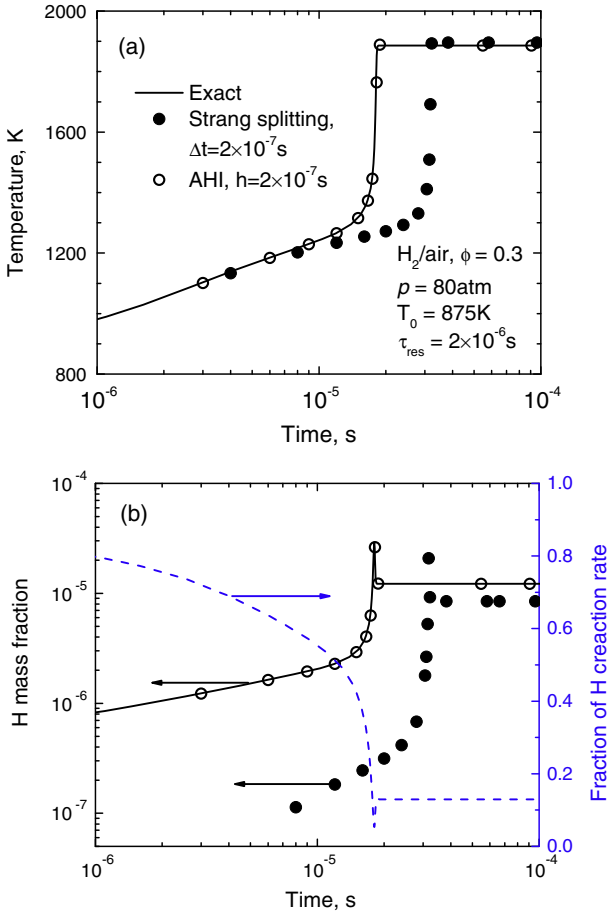

Fig. 13. (a) Temperature, and (b) mass fraction of H and the fraction of H radical creation rate attributed to transport as functions of time in an unsteady PSR for H_2/air with equivalence ratio of $\phi = 0.3$. The inlet stream is fresh mixture of H_2/air at $\phi = 0.3$ and inlet temperature $T_{in} = 875$ K enriched with 0.1% H radical (in mass).

Section 2. The large errors in H concentration subsequently propagate to other quantities and result in significantly delayed ignition. In contrast, H mass fraction is correctly resolved using the AHI method, since the chemical source term and the transport term are integrated together in AHI.

Based on the results for the toy problem and the unsteady PSR for H_2/air, splitting transport from the chemistry integration may result in significant errors in chemistry unless unreasonably small splitting time steps are employed. In this sense transport and stiff chemistry are probably non-split table in general situations, as nonlinearity and radical transportation are frequently involved in combustion.

5. Conclusions

A failing scenario of the operator splitting schemes is identified and demonstrated with a toy problem. In reacting flows with significant radical sources from the transport term, the operator splitting may incur large errors in the radical concentrations by excluding the transport term in the chemistry integration sub-step. Such errors in the radical concentrations may accumulate and lead to significant errors in major species concentrations and global flame responses, particularly when the chemical creation rates of the radicals are relatively low and strong nonlinearity is present in the radical-controlled reactions. Such a scenario is relevant to practical combustion systems such as premixed flame propagation, where the preheat zone receives significant amount of radicals from the neighboring reaction zone through back-diffusion.

The AHI method is proposed as a substitute for the operator-splitting schemes to resolve this issue with improved accuracy while at a comparable or lower computational cost. An efficient criterion in the recent CSP literature is employed to define the timescales of reactions and to subsequently separate the fast and slow reactions and species. The fast chemistry is integrated partial-implicitly while the slow processes, including slow chemistry and transport, are integrated explicitly. The accuracy of the AHI method is demonstrated using auto-ignition of hydrogen/air mixtures. The AHI method shows effective first-order error convergence and is stable using dynamic adaptive fast-slow separation.

The accuracies of the AHI method and the Strang splitting scheme are compared for the toy problem and an unsteady PSR with significant H radical source at inlet. The accuracy of the AHI method is significantly higher than that of the Strang splitting scheme for reasonably small to moderately large integration steps, showing that the transport term should not be excluded from stiff chemistry integration when strong nonlinearity and significant radical transport are involved.

Acknowledgments

This work was supported by the Air Force Office of Scientific Research under Grant FA9550-13-1-0057. The work by Z. Ren was supported by the 111 Project (Ref. No. B13001) and by the Young Thousand Talents Program from the Organization Department of the CPC.

References

[1] T.F. Lu, C.K. Law, Prog. Energy Combust. Sci. 35 (2) (2009) 192–215.
[2] J.H. Chen, A. Choudhary, B. de Supinski, M. DeVries, E.R. Hawkes, S. Klasky, W.K. Liao, K.L. Ma, J. Mellor-Crummey, N. Podhorszki, R. Sankaran, S. S., C.S. Yoo, Comp. Sci. Disc. 2 (2009) 015001.
[3] T.F. Lu, C.K. Law, C.S. Yoo, J.H. Chen, Combust. Flame 156 (8) (2009) 1542–1551.
[4] S.H. Lam, Combust. Sci. Technol. 89 (5–6) (1993) 375–404.
[5] S.H. Lam, Combust. Flame 160 (12) (2013) 2707–2711.
[6] U. Maas, S.B. Pope, Combust. Flame 88 (3–4) (1992) 239–264.
[7] P. Brown, G. Byrne, A. Hindmarsh, SIAM J. Scient. Statist. Comput. 10 (5) (1989) 1038–1051.
[8] M. Caracotsios, W.E. Stewart, Comput. Chem. Eng. 9 (4) (1985) 359–365.
[9] M.J. McNenly, R.A. Whitesides, D.L. Flowers, Proc. Combust. Inst. (2014).
[10] F. Perini, E. Galligani, R.D. Reitz, Combust. Flame 161 (5) (2014) 1180–1195.
[11] F. Perini, E. Galligani, R.D. Reitz, Energy Fuels 26 (8) (2012) 4804–4822.
[12] F. Perini, E. Galligani, G. Cantore, R.D. Reitz, Validation of a Sparse Analytical Jacobian Chemistry Solver for Heavy-Duty Diesel Engine Simulations with Comprehensive Reaction Mechanisms, SAE Technical Paper# 2012-01-1974, 2012.
[13] D.A. Schwer, J.E. Tolsma, W.H. Green, P.I. Barton, Combust. Flame 128 (3) (2002) 270–291.
[14] U.M. Ascher, S.J. Ruuth, R.J. Spiteri, Appl. Numer. Math. 25 (2–3) (1997) 151–167.
[15] U.M. Ascher, S.J. Ruuth, B.T.R. Wetton, SIAM J. Numer. Anal. 32 (3) (1995) 797–823.
[16] J. Frank, W. Hundsdorfer, J.G. Verwer, Appl. Numer. Math. 25 (2–3) (1997) 193–205.
[17] S.Y. Kadioglu, D.A. Knoll, R.B. Lowrie, R.M. Rauenzahn, J. Comput. Phys. 229 (22) (2010) 8313–8332.
[18] S. Ruuth, J. Math. Biol. 34 (2) (1995) 148–176.
[19] G. Marchuk, On the theory of the splitting-up method, in: Proceedings of the 2nd Symposium on Numerical Solution of Partial Differential Equations, SVNSPADE, 1970, pp. 469–500.
[20] N.N. Yanenko, in: The Method of Fractional Steps, Springer-Verlag, New York, 1971.
[21] O.M. Knio, H.N. Najm, P.S. Wyckoff, J. Comput. Phys. 154 (2) (1999) 428–467.
[22] B. Sportisse, J. Comput. Phys. 161 (1) (2000) 140–168.
[23] D.A. Schwer, P. Lu, W.H. Green, V. Semiao, Combust. Theory Model. 7 (2) (2003) 383–399.
[24] D.L. Ropp, J.N. Shadid, C.C. Ober, J. Comput. Phys. 194 (2) (2004) 544–574.
[25] M.A. Singer, S.B. Pope, H.N. Najm, Combust. Theory Model. 10 (2) (2006) 199–217.
[26] G. Strang, SIAM J. Numer. Anal. 5 (3) (1968) 506–517.
[27] R. Speth, W. Green, S. MacNamara, G. Strang, SIAM J. Numer. Anal. 51 (6) (2013) 3084–3105.
[28] Z. Ren, C. Xu, T. Lu, M.A. Singer, J. Comput. Phys. 263 (2014) 19–36.
[29] A.E. Lutz, R.J. Kee, J.A. Miller, Technical Report SAND87-8248, Sandia National Laboratories, 1987.
[30] J. Li, Z.W. Zhao, A. Kazakov, F.L. Dryer, Int. J. Chem. Kinet. 36 (10) (2004) 566–575.
[31] Z. Luo, C.S. Yoo, E.S. Richardson, J.H. Chen, C.K. Law, T. Lu, Combust. Flame 159 (1) (2011) 265–274.
[32] H. Wang, X. You, A. Joshi, S. Davis, A. Laskin, F. Egolfopoulos, C. Law USC Mech Version II. High-Temperature Combustion Reaction Model of H2/CO/C1-C4 Compounds <http://ignis.usc.edu/USC_Mech_II.htm>.